THE LIMIT VALUES AND THE DISTIBUTION OF THREE-DIMENSIONAL PASSIVE EARTH PRESSURES

STANISLAV ŠKRABL

about the author

Stanislav Škrabl
University of Maribor,
Faculty of Civil Engineering
Smetanova ulica 17,
2000 Maribor, Slovenia
E-mail : stanislav.skrabl@uni-mb.si

Abstract

This paper presents a novel approach to the determination of the critical distribution and limit values of three-dimensional passive soil pressures acting on flexible walls following the upper-bound method within the framework of the limit-analysis theory. The method of limit analysis with a set of three-dimensional kinematically admissible hyperbolic translational failure mechanisms is used to determine the critical distribution of the passive pressures along the retaining structure's height. The intensity of the passive pressures is gradually determined with the mentioned translational failure mechanisms in the top-down direction. Thus, the critical distribution, the trust point and the resultant of the passive pressures that can be activated at the limit state for the chosen kinematic model are obtained. The results of the analyses show that the total sum of passive pressures, considering the critical distribution, is lower than the comparable values published in the literature. Furthermore, the trust point of the passive pressure resultant is independent of the friction between the retaining structures and the soil.

keywords

limit analysis, earth pressure, passive pressure, failure surface, soil-structure interaction

1 INTRODUCTION

In geotechnical practice, the results of three-dimensional analyses of passive earth pressures are used to design some anchor systems, to ensure the stability of the foundations of arching and bridging structures, to design embedded caissons and other retaining structures with spaced out vertical supporting elements, etc.

It is only logical that research into passive earth pressures is frequently presented in the literature. The major part of the research deals with 2D stability analyses, while much less attention is paid to 3D analyses. The magnitudes of the earth pressures for the active and passive limit states can be determined by different methods: the limit-equilibrium method (Terzaghi 1943), the slip-line method (Sokolovski 1965) and the limit-analysis method (Chen 1975). In the limit-equilibrium and slip-line methods the static equilibrium and failure conditions are considered, while the expected movements of the retaining structures are not directly considered in the analysis. Generally, a limit analysis serves for determining the upper and lower bounds of the true collapse load by taking into account the supposed movements. The results of the analyses can differ essentially, because they depend on the chosen failure mechanism or the kinematic model of the limit state. Irrespective of the chosen procedure and the method used, the considered static or kinematic model should be in equilibrium when the limit state is reached.

Researchers have used many different methods to determine earth pressures, among them Coulomb (1776), Brinch Hansen (1953), Janbu (1957), Lee and Herington (1972), Shields and Tolunay (1973), Kérisel and Absi (1990), Kumar and Subba Rao (1997), Soubra and Regenass (2000), Soubra (2000), Škrabl and Macuh (2005) and Vrecl-Kojc and Škrabl (2007).

The above-cited, published research mainly considers the 2D problem of passive earth pressures. The results of 3D analyses have been presented only by Blum (1932),

and to a restricted extent. Extensive 3D analyses were treated by Ovesen (1964), who presented the procedure for determining the bearing capacity of different anchor plates based on 2D solutions of passive earth pressures and the results of several experimental studies in 3D conditions.

Soubra and Regenass (2000) published the results of an analysis for determining the 3D passive pressure according to the limit-state analysis using the upper-bound theorem for the translational kinematic admissible multi-block failure mechanism. Duncan and Mokwa (2001) treated the procedures for determining the bearing capacities for anchor plates and presented the results of several experimental studies. Škrabl and Macuh (2005) presented the procedure for a spatial passive pressure analysis based on the hyperbolic kinematic admissible failure mechanism and the upper-bound theorem.

The authors of all the above-mentioned works considered the presumed distribution of passive pressure along the retaining wall height (a triangular distribution for the determination of the self-weight contribution, γ, and a rectangular distribution for the determination of the surcharge contribution, q).

This paper considers the distribution of passive earth pressures along the retaining structure height. The passive pressures distribution is determined numerically with simultaneous analyses of twenty different kinematically admissible translational spatial failure mechanisms.

The results of the analyses show that the resultants of the passive pressures obtained by the presented, proposed procedure give values, lower than those published in the literature for almost all cases; only for the case when $\delta = 0°$ and $\phi \leq 30°$ are the differences minimal, where the values are a little lower or equal to the values presented by Soubra and Regenass (2000), and Škrabl and Macuh (2005).

The application of the upper-bound theorem ensures that the actual values of the passive soil pressures cannot be higher than the values presented in the continuation of this paper.

2 ASSUMPTIONS AND LIMITATIONS

It is a characteristic of passive earth pressures under 3D conditions that they increase as the width of the wall decreases. The value depends on the ground properties and the height/width relationship of the wall. It can be several times higher than the value for 2D cases. The presented geomechanical analysis is based on the following suppositions and limitations:

- the structure discussed is a vertical, flexible wall with an area of $b \cdot h$ (b = width; h = height) and a horizontal backfill,
- the distribution of the passive pressures (p_p) along the wall height is defined by:

$$p_p = e_{p\gamma} \cdot \gamma \cdot (y - y_0) + e_{pq} \cdot q + e_{pc} \cdot c \qquad (1)$$

  where factors $e_{p\gamma}$, e_{pq} and e_{pc} define the distribution of the passive pressures along the height of the vertical wall, and y and y_0 are the coordinates (see Fig. 1),
- the resulting value of the passive earth pressure is defined by:

$$P_p = K^*_{p\gamma} \cdot \gamma \frac{h^2}{2} b + K^*_{pc} \cdot c \cdot h \cdot b + K^*_{pq} \cdot q \cdot h \cdot b \qquad (2)$$

  where $K^*_{p\gamma}$, K^*_{pc} and K^*_{pq} are comparative coefficients of the passive earth pressure due to the soil-weight influence, the cohesion influence, and the surcharge influence, respectively, for a standard, assumed passive pressure distribution,
- the value of the factor $e_{p\gamma}$ at the top of the wall (y=y_0) is equal to 0, its appurtenant values e_{pq} and e_{pc} are determined with a two-dimensional model ($b/h = \infty$) considering the boundary condition for the 3D kinematic admissible failure mechanism,
- the discussed translational failure mechanism is bounded by the log spiral in the region of the retaining wall, and by the hyperbolic surfaces defined by the envelope of the connected hyperbolic half-cones at the lateral sides,
- the lateral surfaces coincide with the margins of the considered retaining wall,
- the backfill is homogenous, the soil is isotropic and considered as a Coulomb material with the associative flow rule obeying Hill's maximal work principle.

3 THE UPPER- AND LOWER-BOUND THEOREMS

The upper-bound theorem ensures that the rate of the work due to the external forces of the kinematic systems in equilibrium is smaller than, or equal to, the rate of dissipated internal energy for all kinematically

admissible velocity fields. The kinematically admissible velocity fields obey strain-velocity compatibility conditions and velocity boundary conditions, as well as the flow rule of the considered materials. The lower-bound theorem for rigid-plastic material using the associative flow rule enables an evaluation of the lower-bound theorem of the true passive earth pressures for each statically admissible stress field that satisfies the equilibrium and stress boundary conditions, and does not violate the yield criteria anywhere. The true value of the failure load is bracketed between both limit values with the expected deviations, which are usually acceptable in geotechnical design.

The presented research considers only the upper-bound theorem of the limit analysis to determine the 3D passive earth pressures using the kinematically admissible velocity field. The solution of the 3D passive earth pressure problem according to the kinematic approach is equivalent to the solution of the limit-equilibrium approach (Mroz and Drescher 1969; Michalowski 1989; Salençon 1990; Drescher and Detournary 1993). The aim of the presented research is to improve on the known lowest values of the upper-bound solutions presented in the literature (Soubra and Regenass 2000, Škrabl and Macuh 2005) using a more exacting passive pressure distribution.

4 TRANSLATIONAL 3D FAILURE MECHANISM

The applied 3D translational failure mechanism represents an extension of the plane slip surface in the shape of a log spiral (see Fig. 1). A very similar 'friction cone' mechanism in the upper-bound analysis of a 3D bearing-capacity problem was used by Michalowski (2001).

Every point along the retaining wall height (1-0, see Fig. 1) is given an exactly defined and kinematically admissible hyperbolic friction cone. The flexionally curved axis and the cross-section of the shaft surface with the plane r-ϑ (see Fig. 1) are:

$$r_*^o = r_* \cdot \cosh((\vartheta - \vartheta_*)\tan\phi) \qquad (3)$$

$$r_*^d = r_* \cdot e^{(\vartheta-\vartheta_*)\tan\phi} \qquad (4)$$

$$r_*^u = r_* \cdot e^{-(\vartheta-\vartheta_*)\tan\phi} \qquad (5).$$

The radius and the centre of the arbitrary half cone in the r-z plane are:

$$R_* = r_* \cdot \sinh\left[(\vartheta - \vartheta_*)\tan\phi\right] \qquad (6)$$

where R_*, r_* and ϑ_* denote the cone diameter in the cross-section of the plane ϑ-z, and the polar coordinates of the apex of the hyperbolic half-cone.

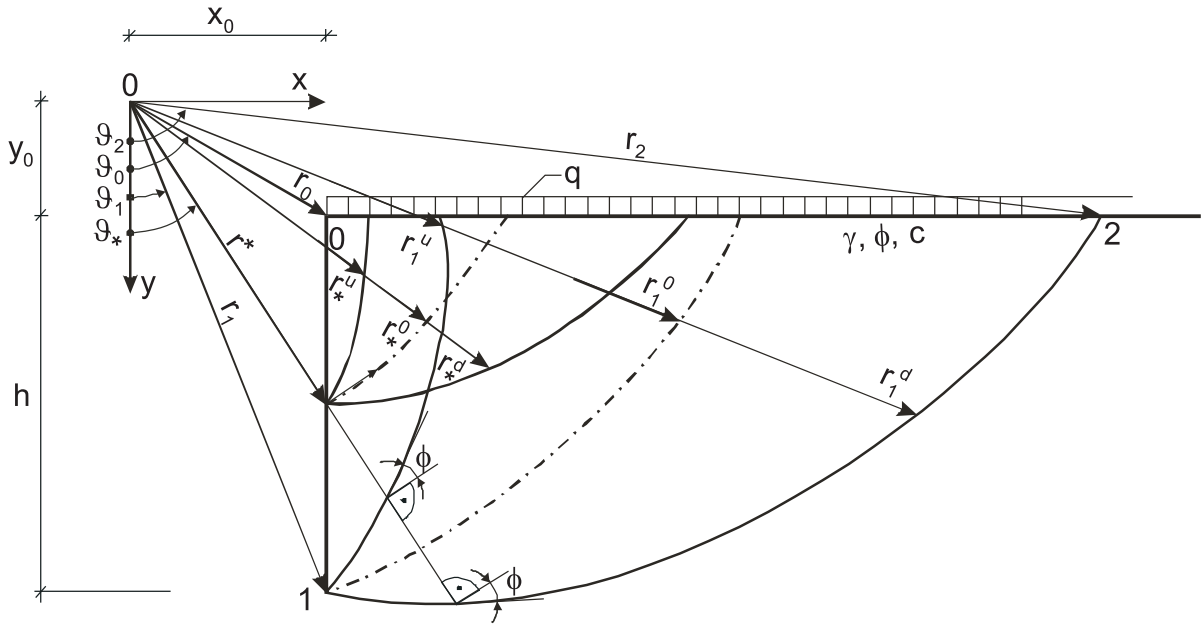

Figure 1. Cross-section of the failure mechanism.

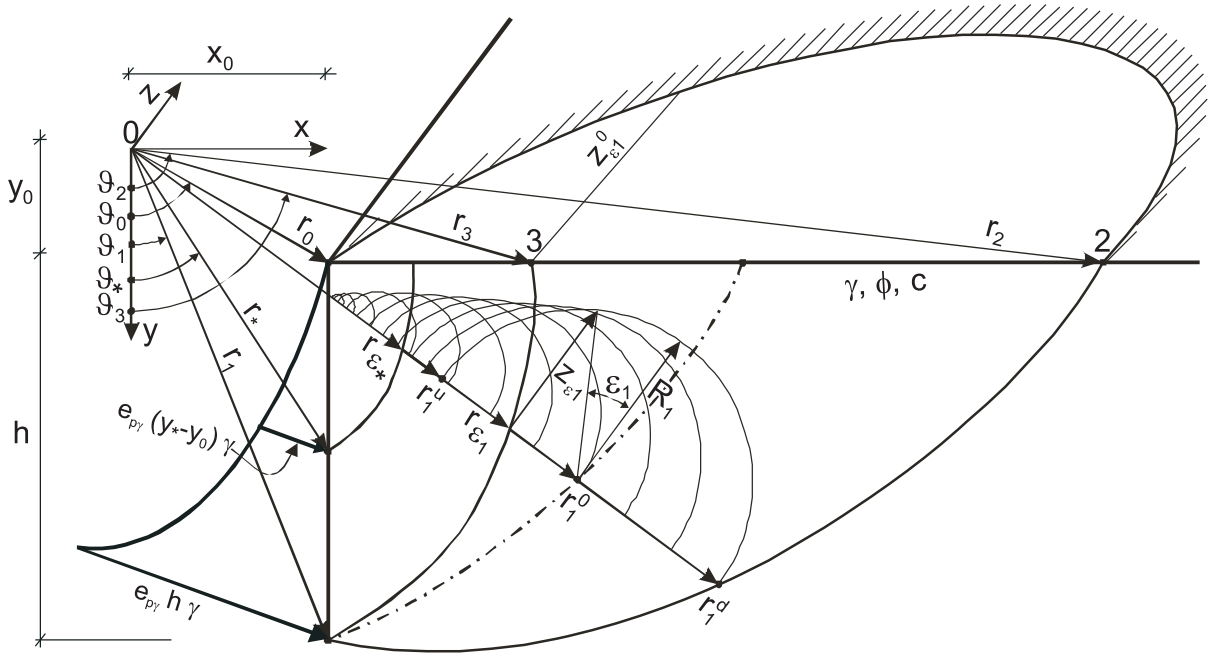

Figure 2. The scheme of the spatial failure mechanism.

All hyperbolic half-cones whose infinite set represents the lateral surface of the failure mechanism are also kinematically admissible when the additional geometry condition is satisfied:

$$\vartheta_0 \leq [\pi/2 - \phi] \qquad (7)$$

which ensures that there exists no half-cone with its apex on the vertical wall (1-0, see Fig. 2) that could intersect the vertical wall under point (r_0, ϑ_0).

Since all the hyperbolic half-cones are kinematically admissible, then using the additional condition (7) the lateral surface, which is the envelope of the infinite set of all half-cones defined by expressions (8), (9) and (10), is also kinematically admissible.

$$r_{\varepsilon_*} = r_* \cosh[(\vartheta - \vartheta_*)\tan\phi] - r_* \sinh[(\vartheta - \vartheta_*)\tan\phi]\sin(\varepsilon_*) \quad (8),$$

$$z_{\varepsilon_*} = r_* \sinh[(\vartheta - \vartheta_*)\tan\phi]\cos(\varepsilon_*) \qquad (9),$$

$$\varepsilon_* = \arcsin(dR_* / dr) = \arcsin\left\{\frac{\tanh[(\vartheta - \vartheta_*)\tan\phi] + \tan\phi\tan\vartheta_*}{1 + \tanh[(\vartheta - \vartheta_*)\tan\phi]\tan\phi\tan\vartheta_*}\right\} (10).$$

Considering $r_* = r_1$ and $\vartheta_* = \vartheta_1$, expressions (8), (9) and (10) define the coordinates of the envelope on the leading half-cone.

The coordinate z_f of the lateral failure surface can be expressed:

$$\forall r \geq \frac{x_0}{\sin\vartheta} \wedge r \leq r_{\varepsilon_1}; \qquad (11)$$
$$z_f = z_{\varepsilon^*} = r_* \sinh[(\vartheta - \vartheta_*)\tan\phi]\cos(\varepsilon_*)$$

$$\forall r \geq r_{\varepsilon_1} \wedge r \leq r_1 e^{(\vartheta - \vartheta_1)\tan\phi}; \qquad (12)$$
$$z_f = z(r,\vartheta) = \sqrt{2rr_1\cosh[(\vartheta - \vartheta_1)\tan\phi] - r^2 - r_1^2}$$

5 WORK EQUATION

The considered failure mechanism on the width b is limited on the left by a vertical wall, on the right by a curved surface in the shape of a log spiral, and above by an even surface on which the surcharge can act. Both lateral surfaces are defined by the curved surfaces of the leading half-cone and the envelope of all the other hyperbolic half-cones (see Fig. 2).

At each point on the so-formed failure surface the normal vector of the surface encloses with the plane *r-z* shear angle ϕ and also defines the direction of the normal stress to the surface (see Fig. 3).

$$dN = \sigma\, dA, \quad dT_\phi = dN\tan\phi, \quad dQ_\phi = \sqrt{dN^2 + dT_\phi^2} \qquad (13)$$

where σ and A denote the normal stress and the area of the lateral surface, and N and T_ϕ denote the resultant

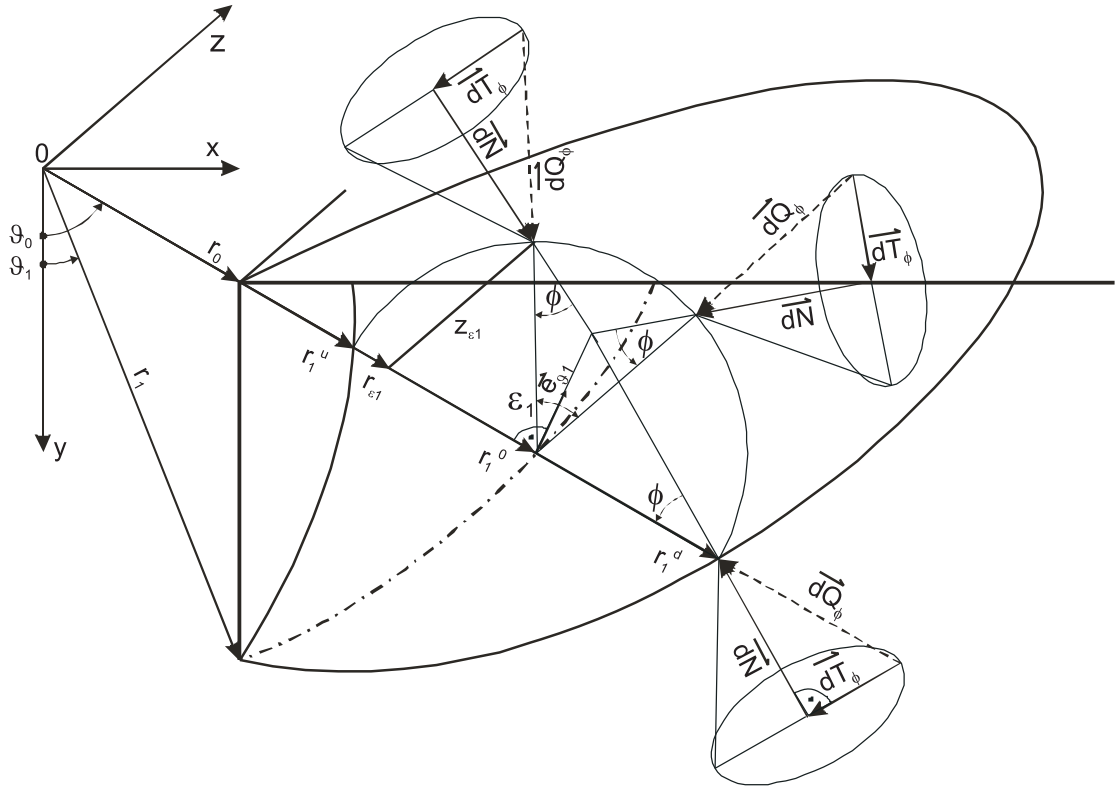

Figure 3. The forces on the failure surface.

values of the normal and the shear-stress components on the spatially formed failure surface.

The shear cones on the failure surface define all the real or admissible directions of the forces dT_ϕ and dQ_ϕ (see Fig. 3). According to the upper-bound theorem the analyses should consider those directions of shear-strength activation that are kinematically admissible and ensure the highest possible value of the passive pressure for the chosen failure mechanism.

The considered spatially formed failure body is certainly symmetrical in the symmetry plane r-ϑ that runs through the centre of the rectangular wall surface, and should be in equilibrium, considering all the forces that act on it.

Certainly, all the forces dQ_ϕ act in the plane r-z, and so they do not cause any momentum around the z axis, which runs through the coordinate system's origin.

Like in the 2D analyses, the equilibrium condition of all the momentums around the z axis is chosen for the work equation. From Fig. 3 it is evident that the maximum possible passive pressures arise when the shear force dT_ϕ acts at each point of the failure surface in a direction that is defined by the cross-section of the normal plane through the centre of the hyperbolic half-cone and the tangent plane to the failure plane through the considered point.

The coefficients of the individual parts of the passive pressure $e_{p\gamma}$ and e_{pq} (let us call them the coefficients of passive pressure distribution) in the 3D problem are not constant along the wall height h. Certainly, they increase non-linearly with increased ratios of b/h. If $\gamma \neq 0$, $\phi \neq 0$, $\delta \neq 0$ and $q = c = 0$ the work equation can be given in the following integral form:

$$\int_{\vartheta_1}^{\vartheta_0} e_{p\gamma}\left(\frac{x_0^3}{\tan\vartheta}-\frac{x_0^3}{\tan\vartheta_0}\right)\left(\frac{\cos\delta\cos\vartheta}{\sin^3\vartheta}-\frac{\sin\delta}{\sin^2\vartheta}\right)d\vartheta-\int_{\vartheta_1}^{\vartheta_0}\int_{x_0/\sin\vartheta}^{r_1 e^{(\vartheta-\vartheta_1)\tan\phi}}(1+2z_f/b)\sin\vartheta\, r^2 dr d\vartheta-$$
$$\int_{\vartheta_0}^{\vartheta_2}\int_{y_0/\cos\vartheta}^{r_1 e^{(\vartheta-\vartheta_1)\tan\phi}}(1+2z_f/b)\sin\vartheta\, r^2 dr d\vartheta=0 \qquad (14)$$

And when $\gamma = 0$, $\phi \neq 0$, $\delta \neq 0$, $q \neq 0$, and c = 0 it can be given in the following integral form:

$$\int_{\vartheta_1}^{\vartheta_0} e_{pq} x_0^2 \left(\frac{\cos\delta\cos\vartheta}{\sin^3\vartheta} - \frac{\sin\delta}{\sin^2\vartheta}\right) d\vartheta - \int_{\vartheta_0}^{\vartheta_2} (1 + 2z_f/b) y_0^2 \frac{\sin\vartheta}{\cos^3\vartheta} d\vartheta = 0 \quad (15)$$

The unknown functions $e_{p\gamma} = e_{p\gamma}(\phi, \delta, b/h)$ and $e_{pq} = e_{pq}(\phi, \delta, b/h)$, which are the minimal possible solutions of the integral expressions (14) and (15) for all real ratios b/h, define the distribution of the passive pressures along the wall height.

The minimum values of $e_{p\gamma}$ and e_{pq} can be determined numerically for an individual in advance for known ratios of b/h. The geometry model (height $h = 1$, unit weight $\gamma = 1$ and ratio b/h) and the soil characteristics (shear angle ϕ and the friction between the soil and the wall δ) were used in our analysis.

6 NUMERICAL ANALYSIS AND RESULTS

The numerical resolving of the integral equations (14) and (15) is performed by dividing the analysed region in the x-y plane into an arbitrary number of triangular and rectangular finite elements. These are suitable for Gauss's numerical integration as well as for the calculation of the integral over the area of the plane $y = y_0$, where one-dimensional Gauss's numerical integration elements (see Fig. 4) are used.

At point $y = y_0$ and when $b/h = \infty$, the factor of the passive pressure distribution is $e_{p\gamma} = 0$, and the appurtenant value of the factor of the passive pressure distribution e_{pq} is determined with a 2D model considering the geometry condition (7).

The values of the passive pressure distribution factors $e_{p\gamma}$ and e_{pq} are determined gradually from the top of the wall downwards for different ratios of b/h ($b/h = \infty$, 100, 75, 50, 25, 20, 16 down to 0.25), as can be seen in Fig. 4. It is assumed in the analysis that the passive pressures increase linearly between the individual calculation points upwards of the wall height. For each calculating point along the wall height there is an exactly determined spatial failure surface, which ensures the smallest possible value of the factors of the passive pressure distribution, $e_{p\gamma}$ and e_{pq}, for the chosen ratio b/h.

In step m of the passive pressure determination, the minimum values of the factors $e_{p\gamma}^0$ to $e_{p\gamma}^{m-1}$ and e_{pq}^0 to e_{pq}^{m-1} are known from the preceding steps. The appurtenant known momentums can be determined with the expressions:

$$f_{p\gamma}^{m-1} = \sum_{i=1}^{m-1} e_{p\gamma}^i (y_i - y_0) \frac{(y_{i+1} - y_{i-1})}{2} \left[\cos\delta \frac{(y_{i-1} + y_i + y_{i+1})}{3} - x_0 \sin\delta\right] \quad (16),$$

$$f_{pq}^{m-1} = e_{pq}^0 \left(\frac{y_1 - y_0}{2}\right)\left[\cos\delta \frac{(y_1 + 2y_0)}{3} - x_0 \sin\delta\right] + \sum_{i=1}^{m-1} e_{pq}^i \frac{(y_{i+1} - y_{i-1})}{2}\left[\cos\delta \frac{(y_{i-1} + y_i + y_{i+1})}{3} - x_0 \sin\delta\right] \quad (17),$$

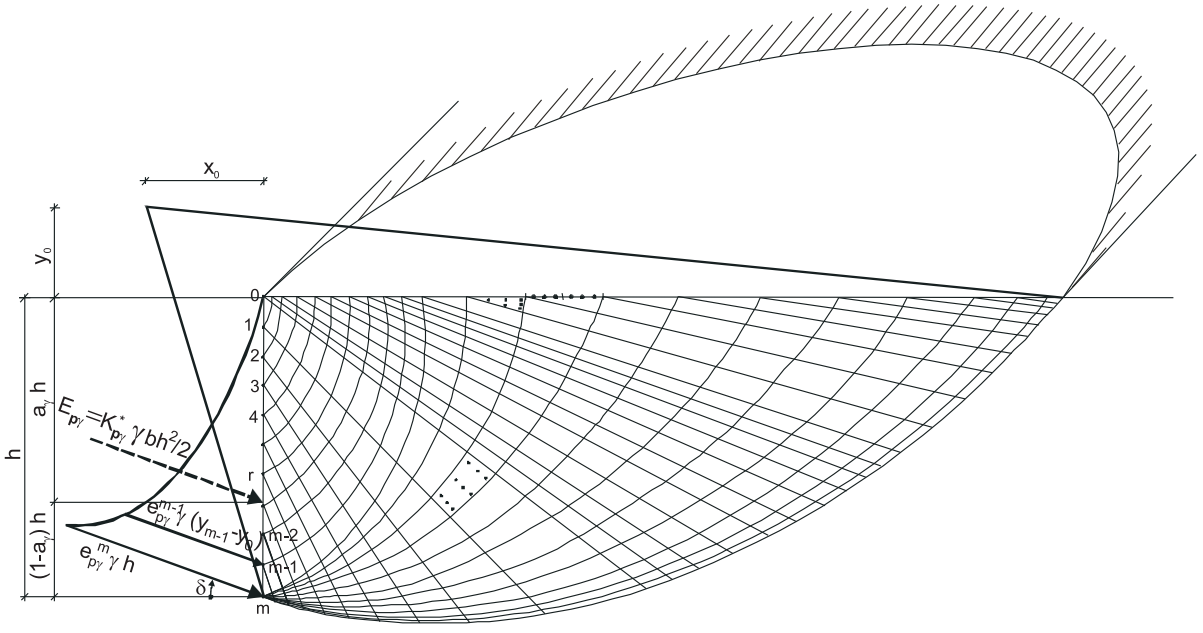

Figure 4. Passive pressure distribution and the scheme of the numerical integration.

$$f_{p\gamma}^{m} = \frac{(y_m - y_{m-1})}{2}\left[\cos\delta\frac{(y_{m-1} + 2y_m)}{3} - x_0\sin\delta\right] \qquad (18),$$

$$f_{pq}^{m} = \frac{(y_m - y_{m-1})}{2}\left[\cos\delta\frac{(y_{m-1} + 2y_m)}{3} - x_0\sin\delta\right] \qquad (19),$$

where $f_{p\gamma}^{m-1}$ and f_{pq}^{m-1} define the momentums of the already known values of the passive pressures, and $f_{p\gamma}^{m}$ and f_{pq}^{m}, the momentums of the passive pressures for $e_{p\gamma}^{m} = 1$ and $e_{pq}^{m} = 1$, according to the origin of the coordinate system *x-y-z*. The appurtenant momentum of the unit weight of the ground ($\gamma = 1$) and the surcharge ($q = 1$), above the failure surface are determined using expressions (20) and (21).

$$g_{p\gamma} = -\sum_{j=1}^{n}\sum_{k=1}^{o} A_{xy}^{j} w_{jk}(1 + 2z_f^{jk}/b) r_{jk}\sin\vartheta_{jk} \qquad (20)$$

where A_{xy}^{j} denotes the area of the triangular or rectangular element *j* in the plane *x-y* (see Fig. 4), w_{jk} is the weight coefficient for Gauss's integration point *k*, z_f^{jk} is the coordinate *z* on the envelope of the hyperbolic half-cones, r_{jk} is the radius of the integration point *k* on element *j* in the plane *x-y*, and ϑ_{jk} is the appurtenant angle of the radius r_{jk}. In the numerical integration of the considered problem in plane *x-y*, 514 rectangular and 42 triangular elements with 9 and 6 Gauss's integration points were used (see Fig. 4).

$$g_{pq} = -\sum_{l=1}^{p}\sum_{k=1}^{r} L_{xy}^{l} w_{lk}(1 + 2z_f^{lk}/b) r_{lk}\sin\vartheta_{lk} \qquad (21),$$

where L_{xy}^{l} denotes the length of a one-dimensional integration element l on the ground surface $y = y_0$ in the plane *x-y* (see Fig. 4), w_{lk} is the weight coefficient for Gauss's integration point *k*, z_f^{lk} is the coordinate *z* of the integration point on the envelope of the hyperbolic half-cones in the plane $y = y_0$, r_{lk} is the radius of the integration point *k* on element *l* in the plane *x-y*, and ϑ_{lk}

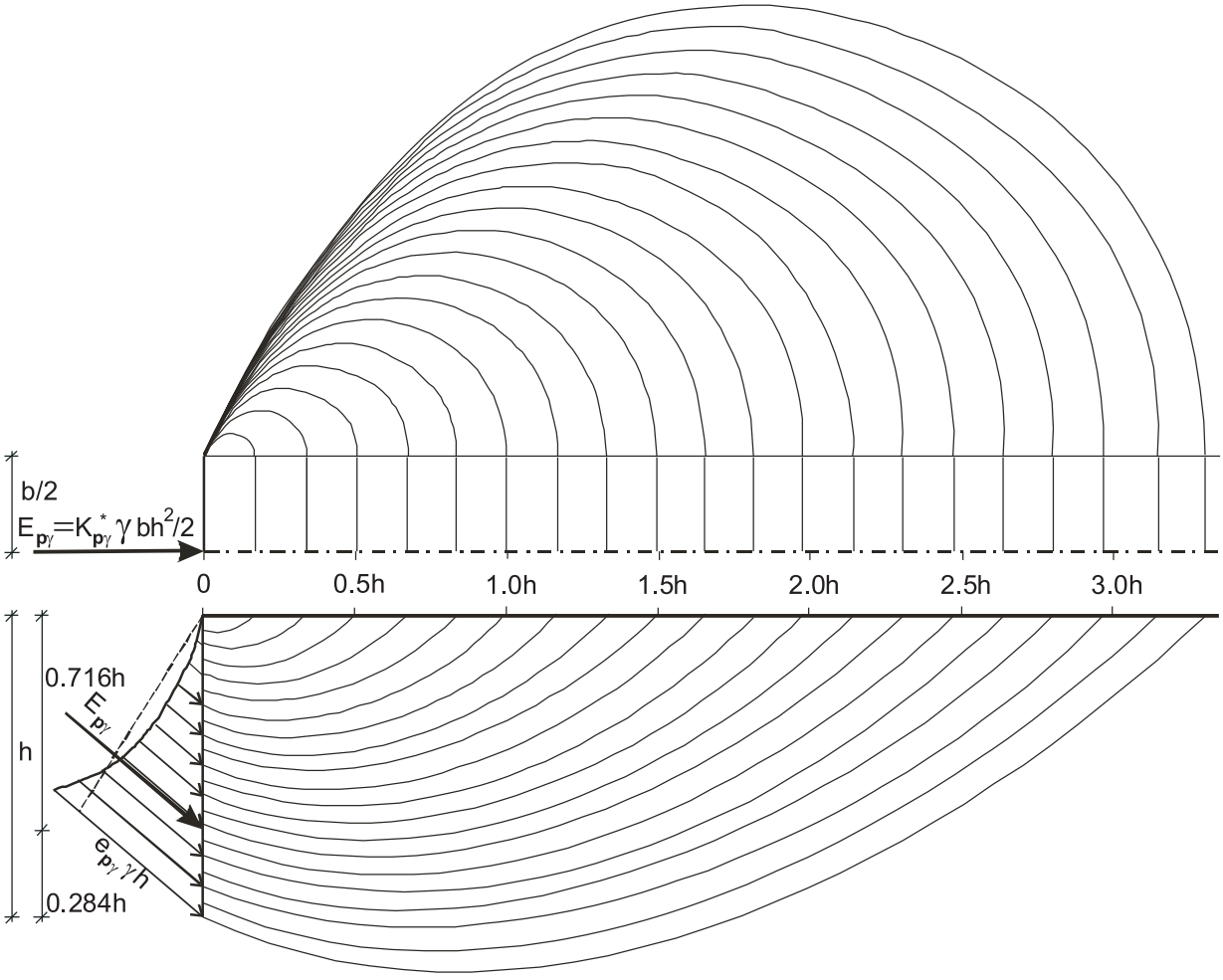

Figure 5. Set of spatial failure surfaces.

is the appurtenant angle of the radius r_{lk}. In the numerical integration of the considered problem in the plane, 42 one-dimensional integration elements with 3 Gauss's integration points were used.

The unknown values of the passive pressure distribution factors are determined using:

$$e_{p\gamma}^{m} = \frac{g_{p\gamma} - f_{p\gamma}^{m-1}}{f_{p\gamma}^{m}}; \quad e_{pq}^{m} = \frac{g_{pq} - f_{pq}^{m-1}}{f_{pq}^{m}} \qquad (22),$$

In the numerical procedure determining the minimal value of the passive pressure distribution factors $e_{p\gamma}^{m}$ and e_{pq}^{m}, the starting failure surface in the optimization procedure is determined with the initial values of the parameters ϑ_1 and ϑ_2, which should satisfy the following boundary conditions:

$$x_0 \geq 0, \quad y_0 \geq 0, \quad \vartheta_0 \geq (\pi/2) - \phi \qquad (23).$$

Mathematical optimization was used to determine the unknown parameters ϑ_1 and ϑ_2 of the critical failure surface, which defines, in the considered calculation step, the minimal value of the unknown factor of the passive pressure distribution, $e_{p\gamma}^{m}$ and e_{pq}^{m}, at the toe of the wall.

The Solver Optimization Tool (Microsoft Excel) with the generalized-reduced-gradient method was used in the minimization process.

The result of the gradual determination of the passive pressure distribution factors from the top of the wall downwards are the numerical values of the factors $e_{p\gamma}$ and e_{pq}, and a set of spatial failure surfaces that are presented in Fig. 5 for the case when $\phi = 40°$ and $\delta/\phi = 1$.

The values of the factors of the passive pressure distribution, $e_{p\gamma}$ and e_{pq}, for different values of ϕ, δ/ϕ and b/h are presented in Figs. 6 and 7.

The values of the comparative passive pressure coefficients, $K_{p\gamma}^{*}$ and K_{pq}^{*}, and the distances of the handling points of the resultants, a_γ, and a_q, from the surface of the backfill soil are presented in Tables 1 and 2.

The values of the handling points are given for individual shear angles and given ratios b/h, where the numerically obtained results for different shear ratios δ/ϕ do not deviate by more than 0.5% from their average value.

The appurtenant values of the substitutive coefficient and the distances of the resultants from the surface of the backfill soil are determined with the expressions (24) to (27).

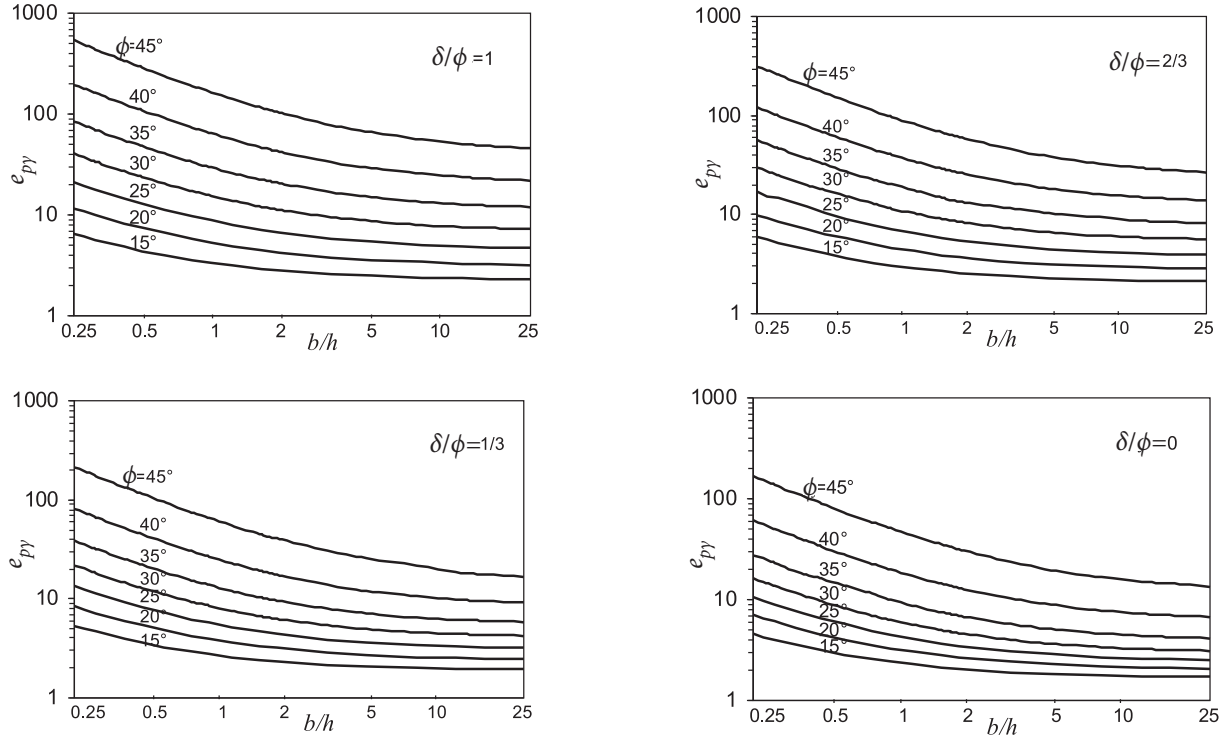

Figure 6. The factors of passive pressure distribution $e_{p\gamma}$ for different values of ϕ, δ/ϕ and b/h.

$$K^{*}_{p\gamma} = \sum_{i=1}^{m-1}(e^{i}_{p\gamma}(y_i - y_0)(y_{i+1} - y_{i-1}) + e^{m}_{p\gamma}(y_m - y_0)(y_m - y_{m-1}) \qquad (24)$$

$$a_{\gamma} = \sum_{i=1}^{m-1}(e^{i}_{p\gamma}(y_i - y_0)(y_{i+1} - y_{i-1})(y_{i-1} + y_i + y_{i+1} - 3y_0)/3) + e^{m}_{p\gamma}(y_m - y_0)(y_m - y_{m-1})(y_{m-1} + 2y_m - 3y_0)/3 \qquad (25)$$

$$K^{*}_{pq} = e^{0}_{pq}(y_1 - y_0)/2 + \sum_{i=1}^{m-1}(e^{i}_{pq}(y_{i+1} - y_{i-1})/2 + e^{m}_{pq}(y_m - y_{m-1})/2 \qquad (26)$$

$$a_q = e^{0}_{pq}(y_1 - y_0)(y_1 - y_0)/6 + \sum_{i=1}^{m-1}(e^{i}_{pq}(y_{i+1} - y_{i-1})(y_{i-1} + y_i + y_{i+1} - 3y_0)/6) + e^{m}_{pq}(y_m - y_{m-1})(y_{m-1} + 2y_m - 3y_0)/6 \qquad (27)$$

In the analyses of the spatial stability problems the theorem of corresponding states (Caquot and Kérisel 1948, Soubra and Regenass 2000) is still valid. The comparative coefficient of the passive earth pressure due to cohesion (K^{*}_{pc}) can be determined by using the comparative coefficient of passive earth pressure due to the surcharge (K^{*}_{pq}).

$$K^{*}_{pc} = \frac{K^{*}_{pq} - 1/\cos(\delta\phi)}{\tan(\phi)} \qquad (28)$$

The values of K^{*}_{pc} for the purely cohesive soil ($c > 0$ and $\phi = 0$) with different ratios of c_a/c and with a centre of gravity of e_{pc} the pressures measured from the top of the wall are given in Table 3.

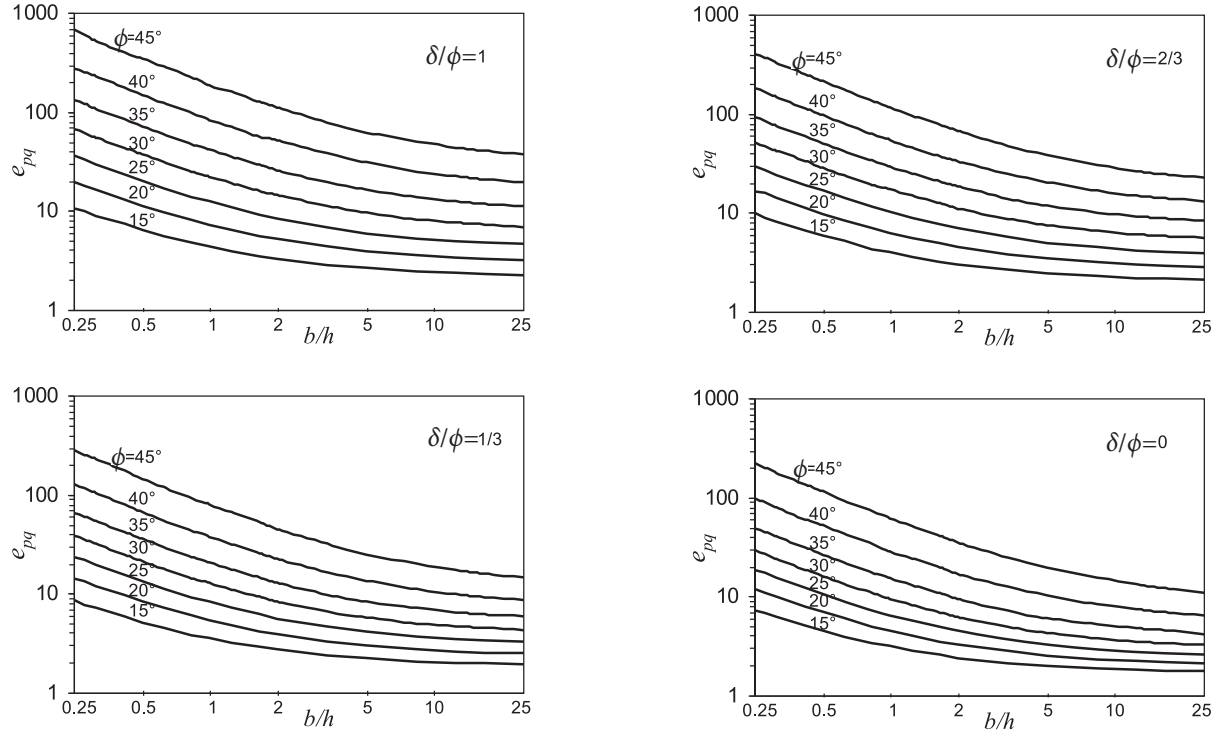

Figure 7. The factors of passive pressure distribution e_{pq} for different values of ϕ, δ/ϕ and b/h.

Table 1. Values of K^{*}_{py} for different values of the parameters ϕ, δ and b/h with the centre of gravity of the e_{py} pressures measured from the top of the wall

b/h	ϕ (deg)	δ/ϕ					center of gravity
		0	1/3	1/2	1/3	1	
0.25	15	3.6279	4.1527	4.3864	4.6365	5.1458	0.712
	20	5.3933	6.4350	7.0004	7.5984	8.8877	0.712
	25	7.9261	10.0117	11.2456	12.6106	15.7108	0.725
	30	11.8711	15.9410	18.5946	21.7237	29.5912	0.730
	35	20.0486	27.6728	33.3372	40.5337	60.4985	0.734
	40	43.0671	57.3693	69.2222	85.9233	139.1175	0.738
	45	116.4677	149.3839	177.6761	220.0038	375.5334	0.741
0.5	15	2.6711	3.0260	3.2012	3.3775	3.7313	0.699
	20	3.7238	4.4311	4.8126	5.2130	6.0592	0.706
	25	5.2089	6.5721	7.3711	8.2474	10.2079	0.712
	30	7.4363	9.9335	11.6437	13.5710	18.3323	0.718
	35	11.9863	16.5711	19.9663	24.2567	36.0095	0.724
	40	24.6495	32.8951	39.7426	49.3782	79.7705	0.729
	45	64.2513	82.5392	98.8063	121.9540	208.4111	0.734
1	15	2.1892	2.4647	2.6014	2.7383	3.0092	0.687
	20	2.8862	3.4211	3.7071	4.0047	4.6270	0.693
	25	3.8439	4.8396	5.4156	6.0425	7.4308	0.698
	30	5.8439	7.0201	8.1663	9.4902	12.6793	0.704
	35	7.9191	11.0232	13.2817	16.1123	23.6998	0.710
	40	15.4367	20.6573	25.0023	31.1047	50.0679	0.716
	45	38.1335	49.1298	58.6535	72.9298	124.8263	0.723
2	15	1.8479	2.1801	2.2961	2.4114	2.6380	0.678
	20	2.4651	2.9099	3.1455	3.3890	3.8937	0.683
	25	3.1579	3.9637	4.4240	4.9214	6.0131	0.687
	30	4.1095	5.5370	6.4305	7.4462	9.8331	0.691
	35	5.9395	8.2498	9.9397	12.0356	17.5319	0.696
	40	10.8269	14.5378	17.6323	21.9686	35.1861	0.702
	45	25.0634	32.4150	38.8084	48.4179	83.0027	0.707
5	15	1.7980	2.0064	2.1091	2.2105	2.4084	0.672
	20	2.2106	2.5986	2.8021	3.0112	3.4411	0.674
	25	2.7423	3.4307	3.8182	4.2341	5.1395	0.676
	30	3.4441	4.6399	5.3717	6.1970	8.1113	0.679
	35	4.7302	6.5872	7.9347	9.5873	13.8072	0.682
	40	8.0584	10.8652	13.2127	16.4877	26.2246	0.686
	45	17.2046	22.3721	26.8925	33.7108	57.8700	0.691
10	15	1.7483	1.9478	2.0456	2.1422	2.3290	0.670
	20	2.1253	2.4935	2.6857	2.8827	3.2865	0.671
	25	2.6034	3.2508	3.6129	4.0005	4.8411	0.672
	30	3.2223	4.3370	5.0128	5.7721	7.5262	0.673
	35	4.3270	6.0335	7.2664	8.7689	12.5571	0.675
	40	7.1344	9.6407	11.7401	14.6610	23.2244	0.677
	45	14.5765	19.0171	22.9160	28.8085	49.4740	0.681
2D	15	1.6984	1.8886	1.9817	2.0736	2.2518	0.667
	20	2.0396	2.3876	2.5686	2.7541	3.1334	0.667
	25	2.4644	3.0696	3.4067	3.7670	4.5479	0.667
	30	3.0000	4.0321	4.6525	5.3492	6.9591	0.667
	35	3.6901	5.4448	6.5993	7.9724	11.3870	0.667
	40	4.5989	7.6224	9.8346	12.6613	20.3076	0.667
	45	5.8284	11.1974	15.6822	21.9144	40.6109	0.667

Table 2. Values of K^*_{pq} for different values of the parameters ϕ, δ and b/h with the centre of gravity of the e_{pq} pressures measured from the top of the wall

b/h	ϕ (deg)	δ/ϕ					center of gravity
		0	1/3	1/2	2/3	1	
0.25	15	4.5768	5.2900	5.6081	5.9280	6.5309	0.609
	20	7.0283	8.4840	9.2341	9.9907	11.5050	0.621
	25	10.7112	13.5556	15.1308	16.8518	20.5128	0.630
	30	16.2767	21.6076	25.0415	28.8780	37.6802	0.637
	35	26.9519	36.2461	42.7186	51.2493	72.8142	0.642
	40	52.6835	68.3932	81.3285	98.5627	151.3097	0.646
	45	116.5809	149.1632	176.9264	217.2506	349.3207	0.650
0.5	15	3.1488	3.5825	3.8054	4.0025	4.4002	0.582
	20	4.5447	5.4631	5.9108	6.3815	7.3299	0.596
	25	6.5956	8.3312	9.2904	10.3297	12.5242	0.608
	30	9.6385	12.8412	14.8706	17.1286	22.2471	0.618
	35	15.4244	20.8022	24.6109	29.5968	41.8059	0.625
	40	29.1399	37.9850	45.2969	55.1065	84.9392	0.632
	45	62.8494	88.6238	95.8063	118.0501	191.9431	0.638
1	15	2.4316	2.7450	2.9041	3.0424	3.3246	0.555
	20	3.3004	3.9297	4.2434	4.5715	5.2181	0.569
	25	4.5344	5.7128	6.3552	7.0497	8.4886	0.581
	30	6.3194	8.4512	9.7630	11.2191	14.4578	0.592
	35	9.6528	13.0803	15.5514	18.7062	26.1839	0.601
	40	17.3562	22.7883	27.2809	33.3902	51.4902	0.610
	45	35.9646	46.3732	55.2288	68.4366	112.5270	0.619
2	15	2.0703	2.3184	2.4440	2.5563	2.7758	0.534
	20	2.6753	3.1633	3.4047	3.6552	4.1404	0.545
	25	3.5038	4.3975	4.8749	5.3812	6.4281	0.555
	30	4.6598	6.2408	7.1807	8.2196	10.4893	0.565
	35	6.7730	9.2194	11.0219	13.1920	18.2517	0.575
	40	11.4902	15.1828	18.2730	22.5430	34.4973	0.585
	45	22.5171	29.1956	34.9820	43.6475	72.5151	0.598
5	15	1.8513	2.0600	2.1639	2.2564	2.4323	0.516
	20	2.2974	2.6965	2.8917	3.0896	3.4692	0.522
	25	2.8854	3.5970	3.9688	4.3579	5.1504	0.529
	30	3.6641	4.9014	5.6070	6.3809	8.0320	0.536
	35	5.0419	6.9032	8.2543	9.7985	13.3404	0.543
	40	7.9825	10.6136	12.8683	16.0172	23.9640	0.551
	45	14.4186	18.8594	22.8019	28.7468	47.8074	0.560
10	15	1.7775	1.9726	2.0678	2.1531	2.3132	0.509
	20	2.1705	2.5382	2.7169	2.8958	3.2362	0.512
	25	2.6793	3.3254	3.6605	4.0075	4.7070	0.516
	30	3.3322	4.4441	5.0746	5.7474	7.1781	0.521
	35	4.4630	3.1341	7.3062	8.6307	11.6245	0.526
	40	6.7878	9.0886	11.0668	13.7561	20.3108	0.531
	45	11.7060	15.4077	18.7082	23.7798	39.2151	0.538
2D	15	1.6984	1.8836	1.9685	2.0050	2.1969	0.500
	20	2.0369	2.3770	2.5400	2.7022	3.0107	0.500
	25	2.4644	3.0468	3.3495	3.6573	4.2786	0.500
	30	3.0000	3.9871	4.5357	5.1180	6.3569	0.500
	35	3.6903	5.3540	6.3516	7.4707	9.9784	0.500
	40	4.5990	7.4305	9.3077	11.5115	16.7775	0.500
	45	5.8284	10.7914	14.4498	19.0443	30.7851	0.500

Table 3. Values of K^*_{pc} for $\phi = 0°$ and different values b/h and c_a/c with center of gravity of e_{pc} pressures measured from the top of the wall.

b/h	K^*_{pc}					center of gravity
	$c_a/c = 0$	$c_a/c = 1/3$	$c_a/c = 1/2$	$c_a/c = 1/3$	$c_a/c = 1$	
0.25	6.9282	7.4720	7.7231	7.9631	8.4156	0.6051
0.50	4.5691	5.0257	5.2356	5.4287	5.7541	0.5854
1.00	3.3302	3.7248	3.8942	4.0439	4.2737	0.5611
2.00	2.6822	3.0314	3.1760	3.3024	3.4925	0.5391
5.00	2.2783	2.5938	2.7217	2.8321	2.9997	0.5192
10.00	2.1402	2.4427	2.5646	2.6693	2.8249	0.5104

Table 4. Comparison of $K^*_{p\gamma}$ and K^*_{pq} with $K_{p\gamma}$ and K_{pq} for different values ϕ, δ/ϕ and b/h.

ϕ (°)	δ/ϕ	$K_{p\gamma}$ (Soubra and Regenass 2000)			$K_{p\gamma}$ (Škrabl and Macuh 2005)			$K^*_{p\gamma}$ (proposed)		
		b/h=0.5	b/h=1.0	b/h=10.0	b/h=0.5	b/h=1.0	b/h=10.0	b/h=0.5	b/h=1.0	b/h=10.0
20	0.5	5.04	3.85	2.75	4.92	3.76	2.69	4.81	3.71	2.69
	1.0	6.99	5.14	3.35	6.35	4.77	3.30	6.06	4.63	3.29
40	0.5	53.74	31.22	14.75	41.55	25.92	11.85	39.74	25.00	11.74
	1.0	131.75	77.02	26.42	90.36	55.48	23.93	79.77	50.07	23.22
ϕ (°)	δ/ϕ	K_{pq} (Soubra and Regenass 2000)			K_{pq} (Škrabl and Macuh 2005)			K^*_{pq} (proposed)		
		b/h=0.5	b/h=1.0	b/h=10.0	b/h=0.5	b/h=1.0	b/h=10.0	b/h=0.5	b/h=1.0	b/h=10.0
20	0.5	6.22	4.45	2.75	6.10	4.35	2.73	5.91	4.24	2.72
	1.0	8.06	5.54	3.17	7.79	5.44	3.27	7.33	5.22	3.24
40	0.5	74.26	43.48	12.82	49.68	29.50	11.33	45.30	27.28	11.07
	1.0	130.19	73.35	21.22	104.80	61.07	21.36	84.94	51.49	20.31

7 COMPARISON WITH EXISTING SOLUTIONS

In the literature only 2D analyses of the soil-pressure-limit values using different approaches are presented, while the research results for 3D cases are very limited. The research results of 3D passive pressure analyses according to the theorem of the upper-bound value have been presented in Soubra and Regenass (2000), and Škrabl and Macuh (2005).

A comparison of the results for the coefficients $K^*_{p\gamma}$ and K^*_{pq} for $\delta/\phi = 0.5$ and 1, $\phi = 20°$ and 40°, $b/h = 0.5$, 1, 10 is presented in Table 4.

A comparison of the results indicates that, particularly at greater shear angles and greater ratios of δ/ϕ, the differences between the values of passive-earth-pressure coefficients for the compared failure mechanisms are the greatest. The coefficient $K_{p\gamma}$ for the proposed translational failure mechanism is up to 11.72% smaller than the same coefficient for the failure mechanism (Škrabl and Macuh, 2005) when $b/h = 0.5$, while the coefficient K_{pq} is up to 18.95% smaller for the same $b/h = 0.5$. For higher ratios of b/h the difference gradually decreases, and when $b/h > 20$ the solutions are almost equal.

8 CONCLUSIONS

This paper presents a procedure for determining 3D passive earth pressures according to the kinematic method of limit analysis. The set of three-dimensional kinematically admissible hyperbolic translational failure mechanisms with lateral surfaces bounded by the envelope of the hyperbolic half-cones is used to determine the critical distribution of passive pressure along a flexible retaining structure's height. The intensity of the passive pressures is gradually determined with the previously mentioned translational failure mechanisms from above, downwards. Thus, the critical distribution, the trust point and the resultant of the passive pressures that can be activated at the limit state for the chosen kinematic model are obtained.

Using the diagrams presented in Figs. 6 and 7 it is possible to determine the actual critical distribution of the passive pressure limit values for any arbitrary practical case (within the frame of given assumptions) that is applicable in geotechnical design.

The results of the numerical analyses indicate that, when considering the upper-bound theorem and the set of three-dimensional kinematically admissible hyperbolic translational failure mechanisms, the passive-earth-pressure coefficients are lower than in the case of the hyperbolic translational failure mechanism and the translational mechanisms published in the literature for $b/h < 10$. The upper-bound values of the comparative passive-earth-pressure coefficients with a calculated pressure distribution are lower than the existing solutions with an assumed pressure distribution obtained using the upper-bound method within the framework of the limit analysis. This means that the classically presumed passive-earth-pressure distribution in 3D analyses is not acceptable, because it can actually not be activated. Furthermore, the trust point of the passive pressures resultant is independent of the friction between the retaining structures and the soil. Therefore, the presented results are applicable in geotechnical practice.

LIST OF SYMBOLS

A_{xy}^{j}	area of triangular or rectangular element j in plane x-y;
b	width of the retaining wall;
c	cohesion;
c_a	adhesion along the soil-structure interface;
e_{pc}	factor of passive earth pressure distribution of the cohesion influence;
$e_{p\gamma}$	factor of passive earth pressure distribution of the soil weight influence;
e_{pq}	factor of passive earth pressure distribution of the surcharge influence;
$f_{p\gamma}^{m}$	momentums of passive pressures for $e_{p\gamma}^{m}=1$
f_{pq}^{m}	momentums of passive pressures for $e_{pq}^{m}=1$
g_{γ}	momentums due to unit weight of the ground;
g_q	momentums due to surcharge loading on the backfill surface;
h	height of the retaining structure;
K_{pc}^{*}	comparative coefficient of passive earth pressure of the cohesion influence;
$K_{p\gamma}^{*}$	comparative coefficients of passive earth pressure of the soil weight influence;
K_{pq}^{*}	comparative coefficient of passive earth pressure of the surcharge influence;
L_{xy}^{l}	length of one dimensional integration element l on the ground surface;
N	resultant value of normal stress component on spatial formed failure surface;
Q_{ϕ}	resultant value of stress on spatial formed failure surface;
$R_{\star}$	cone diameter;
r	polar co-ordinate;
$r_{\star}$	polar co-ordinate of the apex of the curved cone;
$r_{\varepsilon^{*}}$	co-ordinate appurtenant to gradient angle of the envelope;
T_{ϕ}	resultant value of shear stress component on spatial formed failure surface;
w_{jk} w_{lk}	weight coefficients for Gauss's integration point k;
$z_{\varepsilon^{*}}$	co-ordinate appurtenant to gradient angle of the envelope;
$z_{\varepsilon 1}$	co-ordinate of the section of the envelope and the leading cone shaft in plane r-ϑ;
γ	unit weight of the soil;
δ	friction angle at the soil-structure interface;
$\varepsilon 1$	gradient of the envelope in point $r_{\varepsilon 1}$ which is defined in an arbitrary plane r-z;
ϕ	angle of internal friction of the soil;
ϑ	polar co-ordinate;
$\vartheta_{\star}$	polar co-ordinate of the apex of the curved cone.

REFERENCES

[1] Blum, H. (1932). Wirtschaftliche Dalbenformen und deren Berechnung. *Bautechnik*, 10(5): 122-135 (in German).

[2] Brinch Hansen, J. (1953). *Earth Pressure Calculation*, Danish Technical Press, Copenhagen.

[3] Caquot, A., and Kérisel, J. 1948. *Tables for the calculation of passive pressure, active pressure and bearing capacity of foundations*, Gauthier-Villars, Paris.

[4] Chen, W. F. (1975). *Limit analysis and soil plasticity*. Elsevier Scientific Publishing Company, Amsterdam, The Netherlands.

[5] Coulomb, C. A. (1776). Essai sur une application des règles de maximis et minimis à quelques problèmes de statique relatifs à l'architecture. *Mémoire présenté à l'académie Royale des Sciences, Paris*, Vol. 7, 343-382 (in French).

[6] Drescher, A., and Detournay, E. (1993). Limit load in translational failure mechanisms for associative and non-associative materials. *Géotechnique*, London, 43(3): 443-456.

[7] Duncan, J. M. and Mokwa, R. L. (2001). Passive earth pressures: Theories and tests. *Journal of*

Geotechnical and Geoenvironmental Engineering Division, ASCE, 127(3): 248-257.

[8] Janbu, N. (1957). Earth pressure and bearing capacity calculations by generalised procedure of slices. *In Proceedings of the 4th International Conference, International Society of Soil Mechanics and Foundation Engineering*: 207-213.

[9] Lee, I. K., and Herington, J. R. (1972). A theoretical study of the pressures acting on a rigid wall by a sloping earth on rockfill. *Géotechnique*, London, 22(1): 1-26.

[10] Kérisel, J., and Absi, E. (1990). *Tables for the calculation of passive pressure, active pressure and bearing capacity of foundations*. Gauthier-Villard, Paris, France.

[11] Kumar, J., and Subba Rao, K. S. (1997). Passive pressure coefficients, critical failure surface and its kinematic admissibility. *Géotechnique*, London, England, 47(1): 185-192.

[12] Michalowski, R. L. (1989). Three-dimensional analysis of locally loaded slopes. *Géotechnique*, The Institution of Civil Engineering, London, England, 39(1): 27-38.

[13] Michalowski, R. L. (2001). Upper-bound load estimates on square and rectangular footings. *Géotechnique*, The Institution of Civil Engineering, London, England, 51(9): 787-798.

[14] Mroz, Z., and Drescher, A. (1969). Limit plasticity approach to some cases of flow of bulk solids. *Journal of Engineering for Industry*, Transactions of the ASME, 91: 357-364.

[15] Ovesen, N. K. (1964). *Anchor slabs, calculation methods, and model tests*. Bull. No. 16, Danish Geotechnical Institute, Copenhagen: 5-39.

[16] Salençon, J. (1990). An introduction to the yield design theory and its applications to soil mechanics. *European Journal of Mechanics – A/Solids*, Paris, 9(5): 477-500.

[17] Shields, D. H., and Tolunay, A. Z. (1973). Passive pressure coefficients by method of slices. *Journal of the Soil Mechanics and Foundation Division*, ASCE, 99(12): 1043-1053.

[18] Škrabl, S., and Macuh, B. (2005). Upper-bound solutions of three-dimensional passive earth pressures. *Canadian Geotechnical Journal*, Ottawa, 42: 1449-1460.

[19] Sokolovski, V. V. (1965). *Static of granular media*. Pergamon Press, New York.

[20] Soubra, A. H. (2000). Static and seismic earth pressure coefficients on rigid retaining structures. *Canadian Geotechnical Journal*, Ottawa, 37: 463-478.

[21] Soubra, A. H., and Regenass, P. (2000). Three-dimensional passive earth pressure by kinematical approach. *Journal of Geotechnical and Geoenvironmental Engineering Division*, ASCE, 126(11): 969-978.

[22] Terzaghi, K. (1943). *Theoretical soil mechanics*. Wiley, New York.

[23] Vrecl-Kojc, H., and Škrabl, S. (2007). Determination of passive earth pressure using three-dimensional failure mechanism. *Acta Geotechnica Slovenica*, 4(1): 10-23.